The Astrophysical Journal Letters, 930:L11 (7pp), 2022 May 1 https://doi.org/10.3847/2041-8213/ac6879

Multipoint Analysis of the Interaction between a Shock and an ICME-like Structure around 2011 March 22

Mengjiao Xu[1,2], Chenglong Shen[1,2], Can Wang[1], Yutian Chi[1,2], Zhihui Zhong[1], and Yuming Wang[1,2,3]
[1] CAS Key Laboratory of Geospace Environment, Department of Geophysics and Planetary Sciences, University of Science & Technology of China, Hefei, Anhui 230026, People's Republic of China; clshen@ustc.edu.cn
[2] CAS Center for Excellence in Comparative Planetology, University of Science and Technology of China, Hefei, People's Republic of China
[3] Mengcheng National Geophysical Observatory, School of Earth and Space Sciences, University of Science and Technology of China, Hefei, 230026, People's Republic of China
Received 2021 December 6; revised 2022 April 20; accepted 2022 April 20; published 2022 May 4

Abstract

This work reports on the interaction between a fast forward shock and an interplanetary coronal-mass-ejection-like structure (ICMELS) as observed by in situ observations of radially aligned spacecraft. Around 2011 March 22, the Venus EXpress (VEX) and Solar TErrestrial RElations Observatory-A (STEREO-A) were nearly at the same longitude, providing us with an excellent opportunity to study the formation and evolution of the complex structures. The shock and ICMELS investigated in this paper are isolated near Venus, but when they approach STEREO-A, the shock nearly approaches the front edge of the ICMELS and forms a shock–ICMELS complex structure. The maximal magnetic field in the ICMELS increased 2.3 times due to shock compression, according to the observation. The recovery model, which restores the shocked portion of the shock–ICMELS to its uncompressed condition, likewise confirms this improvement. The interaction with the ICMELS, on the other hand, weakens shock 2. The magnetic compression ratio falls from 2.4 at Venus to 2.0 at STEREO-A. This research enables us to have a better physical knowledge of the impacts of the interaction between a shock and an ICME (or ICMELS), which will aid future space weather predictions.

Unified Astronomy Thesaurus concepts: Solar coronal mass ejections (310); Solar-terrestrial interactions (1473); Interplanetary shocks (829)

1. Introduction

Coronal mass ejections (CMEs) are large-scale structures containing mass, kinetic energy, and magnetic flux that are expelled from the Sun into the heliosphere. The interplanetary counterparts of CMEs are called interplanetary CMEs (ICMEs). If a slow CME and a fast CME erupt continuously from the adjacent sites, then fast CMEs will approach and interact with slow CMEs during propagation (Gopalswamy et al. 2001; Shen et al. 2012; Lugaz et al. 2017). In situ observations have shown that the interaction between CMEs can result in many different types of complex structures, including complex jets (Burlaga et al. 2002) and multimagnetic clouds (multi-MC) (Wang et al. 2003b). They might also produce a complex structure called a shock–ICME (S-ICME) structure when the shock driven by the following ICME transmits into the preceding ICME (e.g., Lepping et al. 1997; Wang et al. 2003a; Lugaz et al. 2015). To study the S-ICME structure, a large number of simulations have been carried out (Vandas et al. 1997; Schmidt & Cargill 2004; Xiong et al. 2006; Lugaz et al. 2007; Scolini et al. 2020). These studies found that the interaction may result in the radial compression, acceleration, and heating of the ICME, as well as the weakening, dissipation, or merging of the shock.

ICMEs are known to be the major sources of geomagnetic storms (Gonzalez et al. 1994; Zhang et al. 2007; Shen et al. 2017). This is largely because they often contain a long-lasting intense southward magnetic field component (B_s) (Tsurutani et al. 1988; Kamide et al. 1998). As the interaction between the shock and the ICME would enhance the magnetic field intensity in the interaction structures, S-ICMEs are thought to be more geoeffective than individual ICMEs (Shen et al. 2017, 2018; Srivastava et al. 2018; Scolini et al. 2020; Xu et al. 2019). In addition, S-ICMEs can lead to a new type of double-dip storm unlike the classical double-dip storm caused by different B_S structures in the shock sheath and ICME. In such storms, both dips are due to the Bz structure in ICMEs, as indicated by previous studies (Farrugia et al. 2006; Gopalswamy et al. 2015).

To quantitatively study the enhancement of B_s caused by S-ICME interaction, Wang et al. (2018) put forward a recovery method that relates the magnetic field, plasma velocity, and density in the shocked part of the ICME to the uncompressed state by applying the Rankine–Hugoniot jump conditions at the shock surface. However, as Wang et al. (2018) mentioned, this method of recovering the shocked structure is highly ideal. It assumes that the shock properties remain the same after it enters the ICME. However, due to the relatively large Alfvén speed in ICMEs, shocks would weaken or even dissipate during the propagation inside ICMEs (Vandas et al. 1997; Lugaz et al. 2007). Besides, the shocked part of the ICME would recover (Xiong et al. 2006). Therefore, multipoint observations are required to gain a more straightforward comprehension of the effect of S-ICME interaction on shock properties and the magnetic field in ICMEs.

Accurate and routine determination of CME–CME interaction is feasible with the launch of the Solar Terrestrial Relations Observatory (STEREO; Kaiser et al. 2008), which provided us with the opportunities to track CMEs continuously between the Sun and Earth from multiple viewpoints. Nevertheless, the

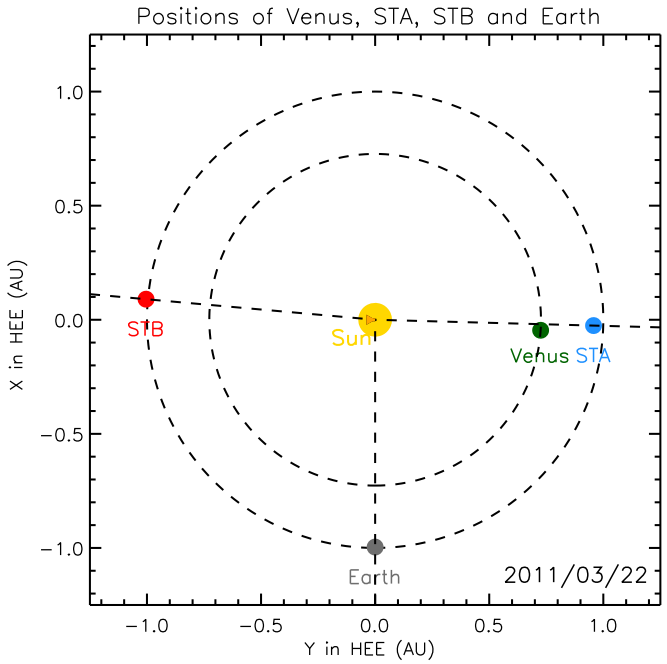

Figure 1. Positions of Earth, STEREO-A, STEREO-B, and Venus on March 22, 2011.

current understanding of the interacting CME structure is limited by the lack of multipoint in situ observations of the magnetic field and solar wind parameters during its propagation. Although recent planetary exploration missions such as MErcury Surface, Space ENvironment, GEochemistry, and Ranging (MESSENGER), Venus EXpress (VEX; Svedhem et al. 2007; Titov et al. 2006), Mars Atmosphere and Volatile EvolutioN (MAVEN), and Tianwen, as well as the Parker Solar Probe (PSP) and solar orbiter, have made it possible to study the evolution of interacting CME structures using multipoint in situ observation, there is not much research on events well observed by multiple spacecraft with different radial distances (Good & Forsyth 2016; Janvier et al. 2019; Salman et al. 2020).

This study analyzes the interaction of two ICME events observed successively by VEX and STEREO-A around 2011 March 22. In Section 2, the in situ observation of the event at Venus and STEREO-A is presented. The effects of the S-ICME interaction on ICME and shock parameters are discussed in Section 3. In the last section, a conclusion is provided and a short discussion follows.

2. Observations of the Complex Structure

On 2011 March 22, STEREO-A is hit by a fast and large Interplanetary Coronal Mass ejection (ICME), which triggers a large solar energetic particle event (with energies exceeding 400 MeV) (Rouillard et al. 2012). According to the in situ observation of STEREO-A, the shock driven by this ICME is positioned in an ICME-like structure (ICMELS), implying a possible S-ICME complex structure. Fortunately, during that time, Venus was roughly at the same longitude as STEREO-A, allowing us to combine observations from VEX and STEREO-A to track the evolution of this complex structure and analyze the impact of the interaction process. The relative positions of Earth, STEREO, and Venus on 2011 March 22 are depicted in Figure 1. Venus and STEREO-A are almost radially aligned, with a separation angle of only 3°. In the following sections, we will introduce the observations of VEX and STEREO-A individually, as well as explore the effects of the S-ICME interaction on ICME and shock parameters.

2.1. The Observation at Venus

VEX was launched in 2005 November and was in service from April 2006 until the end of 2014. As VEX orbited the planet, it spent enough time in the solar wind to detect shocks and ICMEs. On average, there is one magnetospheric crossing per day, lasting about 2.5 hr. Although the VEX payload included the Analyser of Space Plasmas and Energetic Atoms (ASPERA-4) (Barabash et al. 2007), there are only scattered measurements of pure solar wind plasma. Therefore, the magnetic field data used to identify ICMEs and shock crossings at the Venusian orbit (0.72 au) were recorded by the fluxgate magnetometer (MAG) onboard VEX (Zhang et al. 2006).

The left panels of Figure 2 show the magnetic field measurements made by VEX from March 22 to 24. Panel (a) presents the time–intensity profile of the total magnetic field strength, $|B|$. Panels (b)–(d) show the variations of B_R, B_T, and B_N over time in RTN coordinates. Panels (e) and (f) display the changes in elevation angle, θ, and azimuthal angle, ϕ, of the magnetic field vector, respectively. Two magnetic structures (gray and yellow shaded regions) and two fast forward shocks (vertical black line and orange line) can be recognized.

The first magnetic structure (gray shaded region) is pretty short. According to the figure, it begins at 22:11 on March 21 and ends with VEX's entry into the magnetosphere at about 02:30 on March 22, lasting approximately 4.3 hr. This somewhat underestimates the length of the structure because the interplanetary observation is interrupted when VEX in the magnetosphere. When VEX returns to the interplanetary space at 04:40, the observed magnetic field is significantly different from its previous direction, so it is no longer the same structure as before. That is to say, the rear boundary could be at any time when the VEX is in the magnetosphere and the duration of this magnetic structure may range from 4.3 hr to 6.5 hr. The magnetic field in the structure rotates smoothly, but the maximum intensity $|B|$ in it is only 12.3 nT, which is much lower than the average value of 28 nT of the ICMEs at VEX (Salman et al. 2020). Based on the above characteristics, we consider this magnetic structure as an ICME-like structure (ICMELS) that exhibits some classical ICME signatures but has weak magnetic field strength and short duration (Kilpua et al. 2012). There is a fast forward shock (black vertical line) about 13 hr ahead of the ICMELS. Hereinafter, it will be referred to as shock 1. Because the distance between shock 1 and the following ICMELS is very long, about two to three times longer than the duration of the ICMELS, it cannot be taken for granted that shock 1 is driven by the ICMELS. It is possible that shock 1 is a driverless shock and the ICMELS is an unrelated structure. Therefore, we do not judge and focus on the relationship between them. Based on the shock catalog of Wang et al. (2021), in which the parameters of VEX-observed shocks have been fitted with the magnetic coplanarity method, the normal direction of shock 1 is [0.94,0.16,0.31] in RTN coordinates, and its magnetic compression ratio is 1.7.

The second magnetic structure (yellow shaded region) is relatively larger and stronger. It is a typical ICME event characterized by enhanced magnetic field strength and smooth magnetic field rotation. The ICME begins with the feature of an increase in magnetic field strength at 17:28 UT on March 22

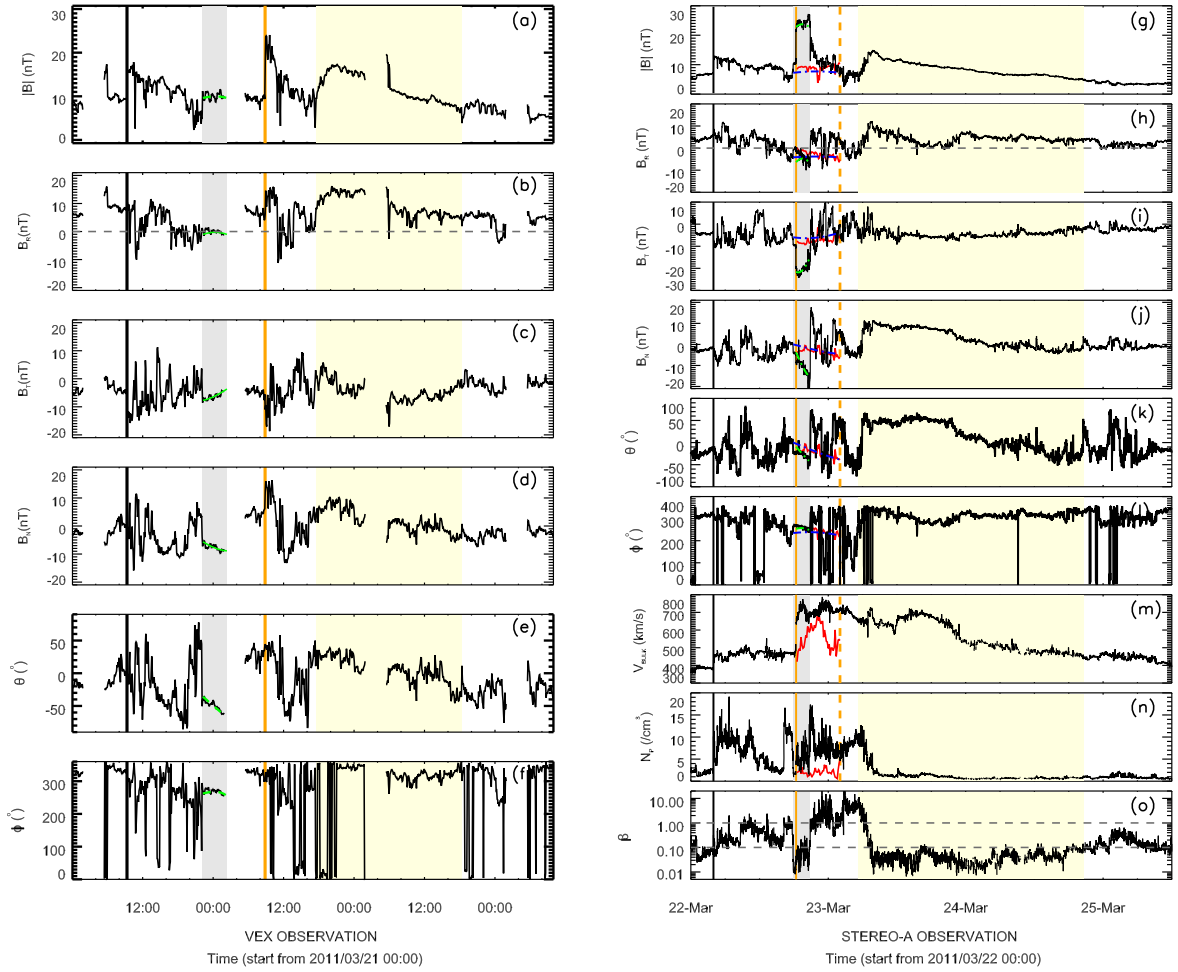

Figure 2. Left: magnetic field measurements by VEX from 2011 March 21 to 24. The overlying green dashed lines are the fitting results of the force-free model. The gray and yellow shaded regions represent an ICME-like structure (ICMELS) and an ICME, respectively. The vertical black line and orange line indicate two fast forward shocks. Right: the black solid curves are the magnetic field and solar wind measurements by STEREO-A from 2011 March 22 to 25. The red solid lines between the orange solid vertical line and the orange dashed vertical line in panels (g)–(n) represent the recovered states of the S-ICMELS complex structure. The overlaid green and blue dashed lines in panels (g)–(l) show the fitting results of the force-free model. The ICMELS and the ICME are indicated by gray and yellow shaded regions. The vertical black and orange solid lines indicate the two fast forward shocks, and the vertical orange dashed line shows the recovered trailing edge of the ICMELS.

and ends with the feature of a spike of θ to a positive value at 18:20 UT on March 23. The maximum magnetic field strength in it is 18.3 nT. This ICME drives a fast forward shock (hereinafter referred to as shock 2), which is marked by the orange vertical line in the figure.

The normal direction of shock 2 is [0.37, 0.90, 0.22] in RTN coordinates, which is very unusual. This may result from the failure of the magnetic coplanarity method to fit shock 2 very well. We will discuss it in Section 4. The magnetic compression ratio of shock 2 is 2.4, larger than the average level of shocks near Venus. In addition, although the shock speed cannot be directly calculated due to the lack of plasma observations by VEX, using the arrival times of the shock waves at STEREO-A and VEX, we can roughly estimate that the velocity of shock 2 should be no less than 1462 km s^{-1}. All these findings indicate that shock 2 is fast and strong, having the potential to propagate for a long time in the ICMELS.

At Venus, shock 2 and the ICMELS are still independent, allowing us to see their properties before the interaction. Hence, we reconstruct the ICMELS here based on Lundquist's constant-α force-free field solution (Lundquist 1950) to see its properties before the shock's impact. Measurements of the magnetic field are used to fit the flux rope in this model.

The fitting results of ICMELS are represented in Figure 2 by green dashed lines. Table 1 shows some of the most relevant fitting parameters acquired by the model, such as the magnetic field strength at the axis of the flux rope (B_0), the orientation of the axis (elevation angle θ and azimuthal angle ϕ in RTN coordinates), and the closest approach of the observational path to the axis of the flux rope(d). The fitted d is 0.96 in this case, indicating that just the outer shell of the structure, not the inner core, has been detected. Furthermore, the fitted B_0 is 18.5 nT, which is significantly higher than the observed value, implying that the magnetic field strength of the ICMELS is actually large, but because VEX just crosses the edge of the ICMELS, we do not detect any significant magnetic intensity enhancement.

2.2. The Observation at STEREO-A

After about one day, the ICMELS/ICME and shocks reach STEREO-A. At STEREO-A, shock 2 has already penetrated into the ICMELS and formed a shock–ICMELS complex

Table 1
Parameters of the Shock–ICMELS Complex Structure

	ICMELS					Shock 2	
	Observations		Fitting Parameters			$\hat{n}$[f]	r_B[g]
	B_{max}[a]	Duration[b]	B_0[c]	(θ, ϕ)[d]	d[e]		
At Venus	12.3	4.3–6.5	18.5	(−5, 356)	0.96	[0.37, 0.90, 0.22]	2.4
At STEREO-A	27	2.9	44	(−7, 345)	0.96	[0.98, 0.02, −0.22]	2.0
Recovered states	10.1	8.2	14.6	(−15, 325)	0.93	⋯	⋯

Notes.
[a] Maximum observed magnetic field strength, in units of nT.
[b] Duration of ICMELS, in units of hr.
[c] Magnetic field strength at the axis of the flux rope, in units of nT.
[d] Elevation angle (θ) and azimuthal angle (ϕ) of the axis of the flux rope in RTN coordinate.
[e] The closest approach of the observational path to the axis of the flux rope, in units of the radius of the cross section of the flux rope.
[f] Normal direction of the shock in RTN coordinate.
[g] Magnetic compression ratio.

structure. The right panels of Figure 2 show the observation of STEREO-A during the period from 2011 March 22 to March 25. The black curves in panels (g)–(o) show the time–intensity profile of the total magnetic field strength $|B|$, three magnetic field components in RTN coordinates, the elevation and azimuthal angle of the magnetic field vector, solar wind speed, proton number density, and plasma β. Similar to the left part, the ICMELS and the ICME are indicated by gray and yellow shaded regions, and the two shocks are shown by black and orange solid vertical lines. A quick glance at the figure reveals how far shock 2 has propagated in the ICMELS. The front edge of the ICMELS is barely 0.5 hr before shock 2. Such complex structures are uncommon. Because of the large upstream magnetosonic speeds, most shocks in S-ICME events are located toward the ICME's rear boundary (Lugaz et al. 2015).

The identified ICME interval from the STEREO-A observation is shown by the yellow shaded region. For consistency, we use the magnetic field enhancement and the spike of θ to mark the front and rear boundaries. At STEREO-A, the ICME lasts from 05:15 UT on March 23 to 20:38 UT on March 24. Comparing the observation by STEREO-A and VEX, we find that its duration increases by a factor of 1.6. In addition, as a result of the expansion, its maximum magnetic field strength decreases from 18.3 nT at Venus to 14 nT at STEREO-A. The ICMELS, on the other hand, is shortened due to shock compression. Its duration at STEREO-A is approximately 2.9 hr, which is 1.5–2.2 times shorter than that at Venus. Besides, measurements of the ICMELS show a very strong magnetic field, reaching 27 nT at its maximum. This is contrary to what has been observed at VEX, where the maximum magnetic field strength is only 12.3 nT. Because of the compression of shock 2, the magnetic field intensity of ICMELS has not only not decreased during the propagation but also increased 2.3 times.

To calculate the parameters of the two shocks at STEREO-A, we adopt the mixed-mode method to fit the shock (Abraham-Shrauner & Yun 1976). The fitted normal directions of shock 1 and shock 2 are [0.95, 0.31, 0.02] and [0.98, 0.02, −0.22] in RTN coordinate,s and their speeds are 445 km s^{-1} and 780 km s^{-1}. The magnetic compression ratios of shock 1 and shock 2 are 1.7 and 2.0, respectively. For consistency, we further calculate the shock normal directions with the magnetic coplanarity method, yielding normal directions of [0.96, 0.29, 0.03] and [0.56, 0.33, −0.8] in RTN coordinates for shock 1 and shock 2, respectively. For shock 1, the normal direction fitted by the mixed-mode method and magnetic coplanarity method is essentially the same. Shock 2, on the other hand, is quite different.

To quantitatively check the effect of shock 2 compression on the ICMELS, we use the modal developed by Wang et al. (2018) to recover the shocked part of the ICMELS to the uncompressed state. This model relates the magnetic field, plasma velocity, and density in the sheath region to the uncompressed states by applying the Rankine–Hugoniot jump conditions at the shock surface. Treating the shocked part of the ICMELS as the downstream of the shock, the parameters in the shock upstream, that is, the recovered uncompressed state, can then be calculated. In the right panel of Figure 2, the red dashed curves in panels (g)–(n) between the orange solid line and the orange dashed line show the recovered parameters. The orange dashed vertical line represents the recovered rear boundary of the ICMELS. According to the recovered results, the peak value of the magnetic field strength is only 10.1 nT and the duration is 8.2 hr. In other words, if there is no shock compression, the ICMELS will last 1.4–1.9 times longer at STEREO-A than at VEX, and the maximum magnetic field intensity will be roughly 0.8 times as great as that at VEX. It should be noted that this method is ideal. It assumes that after entering the ICME, the shock parameters will remain unchanged. In practice, however, the shock may decelerate and the compression ratio may decrease.

We apply force-free fitting on the shocked part of the S-ICMELS (the observation between shock 2 and the rear boundary of the ICMELS) as well as the recovered uncompressed state of the ICMELS (the recovered state between the observed front boundary and the recovered rear boundary of the ICMELS). Green and blue dashed curves represent the fitting results, respectively. Both fitting results, as shown in the figure, mirror the magnetic field observation. The fitting parameters are listed in Table 1. The axis orientation (θ and ϕ) and the closest approach of the observational path to the axis (d) fitted from both observed data and recovered states are all similar to those of the ICMELS at VEX. The observed ICMELS at STEREO-A has a fitted B_0 of 44 nT, which is nearly 2.4 times greater than that at VEX. In contrast, the fitted B_0 of the recovered states is just 14.6 nT, which is about 1.3 times smaller than that at VEX. The changes in the fitted magnetic field strength are consistent with the observation, as can be shown.

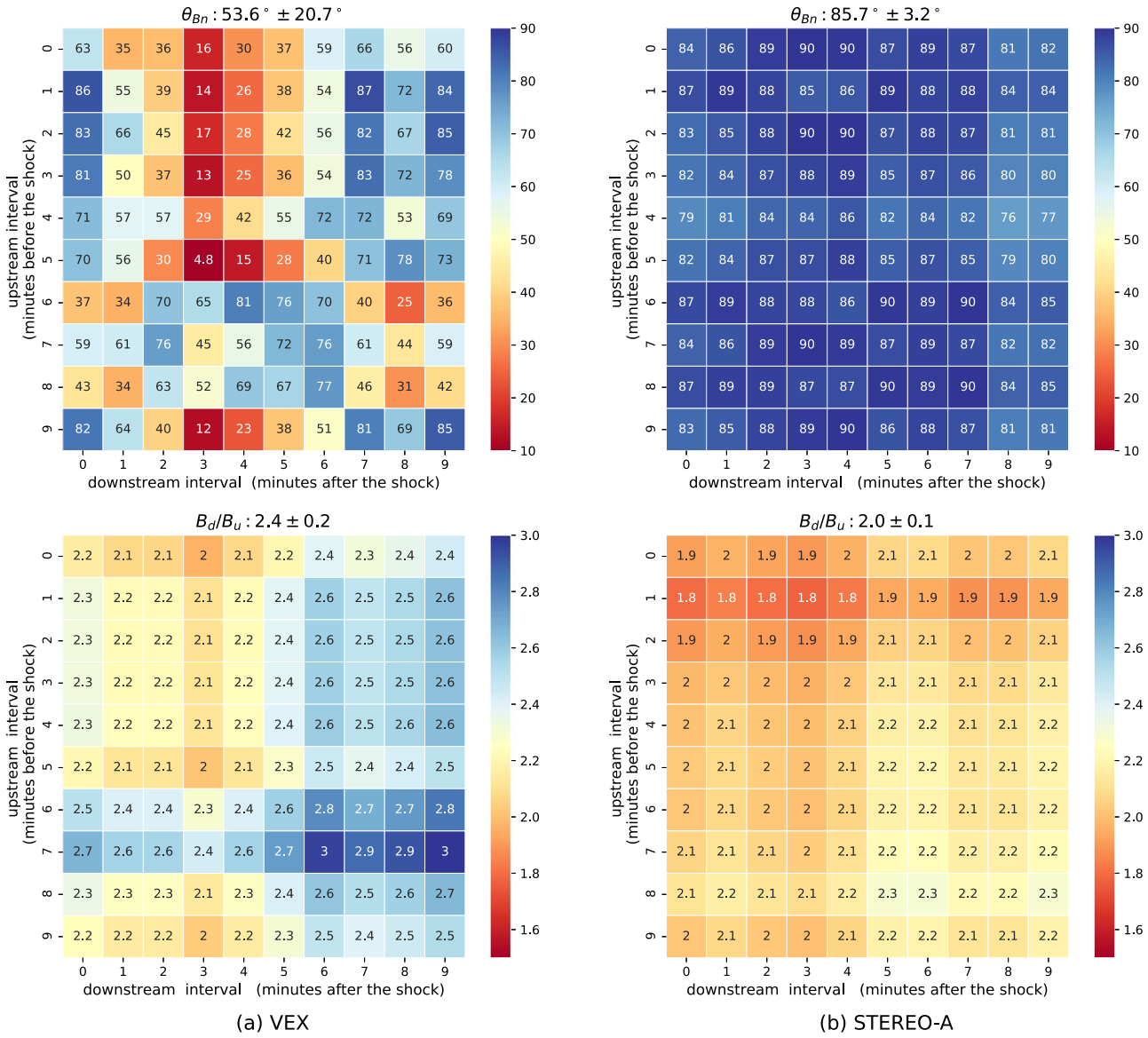

Figure 3. Left: the distribution of the calculated shock directions θ_{BN} (top) and magnetic compression ratios (bottom) of shock 2 at VEX by selecting different upstream and downstream intervals. The shock direction θ_{BN} is fitted with the magnetic coplanarity method. Right: the distribution of the calculated shock directions θ_{BN} (top) and magnetic compression ratios (bottom) of shock 2 at STEREO-A by selecting different upstream and downstream intervals. The shock direction θ_{BN} is fitted with the mixed-mode method. In all subplots, the horizontal coordinate represents the selected downstream intervals, the time period (in minutes) after the shock. The ordinate represents the selected upstream intervals, the time period (in minutes) before the shock.

3. Effects of the Shock–ICME Interaction

In this section, we will investigate the effects of shock–ICMELS interaction by comparing the properties of shock 2 and the ICMELS at Venus and STEREO-A. The parameters of shock 2 are presented in the last two columns of Table 1, including shock normal direction ($\hat{n}$) and magnetic compression ratio (r_B). From Venus to STEREO-A, the intensity of the shock weakened significantly, with the magnetic compression ratio decreasing from 2.4 to 2.0. It is common for shock compression ratios to decrease during propagation, but given that in this case the magnetic compression ratio of shock 1 has not decreased from Venus to STEREO-A and that statistical studies have revealed that the average shock magnetic compression ratio only declines from 2.1 ± 0.6 at Venus (Wang et al. 2021) to 2.0 ± 0.7 at 1 au (Kilpua et al. 2015), we can infer that the weaken of shock 2 is more severe. The entry of shock 2 into the ICMELS during propagation may be the reason for the substantial decrease in shock intensity. Because the magnetosonic speed inside the ICMELS is much higher than that in the background solar wind, shock 2 is weakened more significantly.

Besides, we can find that the normal direction of shock 2 changes a lot from VEX to STEREO-A. At VEX, the magnetic coplanarity method is applied to fit the shock, yielding a normal direction of [0.37,0.90,0.22] in RTN coordinates. At STEREO-A, both the magnetic coplanarity method and the mixed-mode method are used to fit the shock, and the achieved normal directions are [0.56,0.33, −0.8] and [0.98,0.02, −0.22] respectively. At STEREO-A, the shock normal directions fitted by the two methods are quite different. In addition, neither of them matches up to the shock normal direction fitted by the magnetic coplanarity method at VEX. This may have to do with the interaction between shock 2 and the ICMELS, which

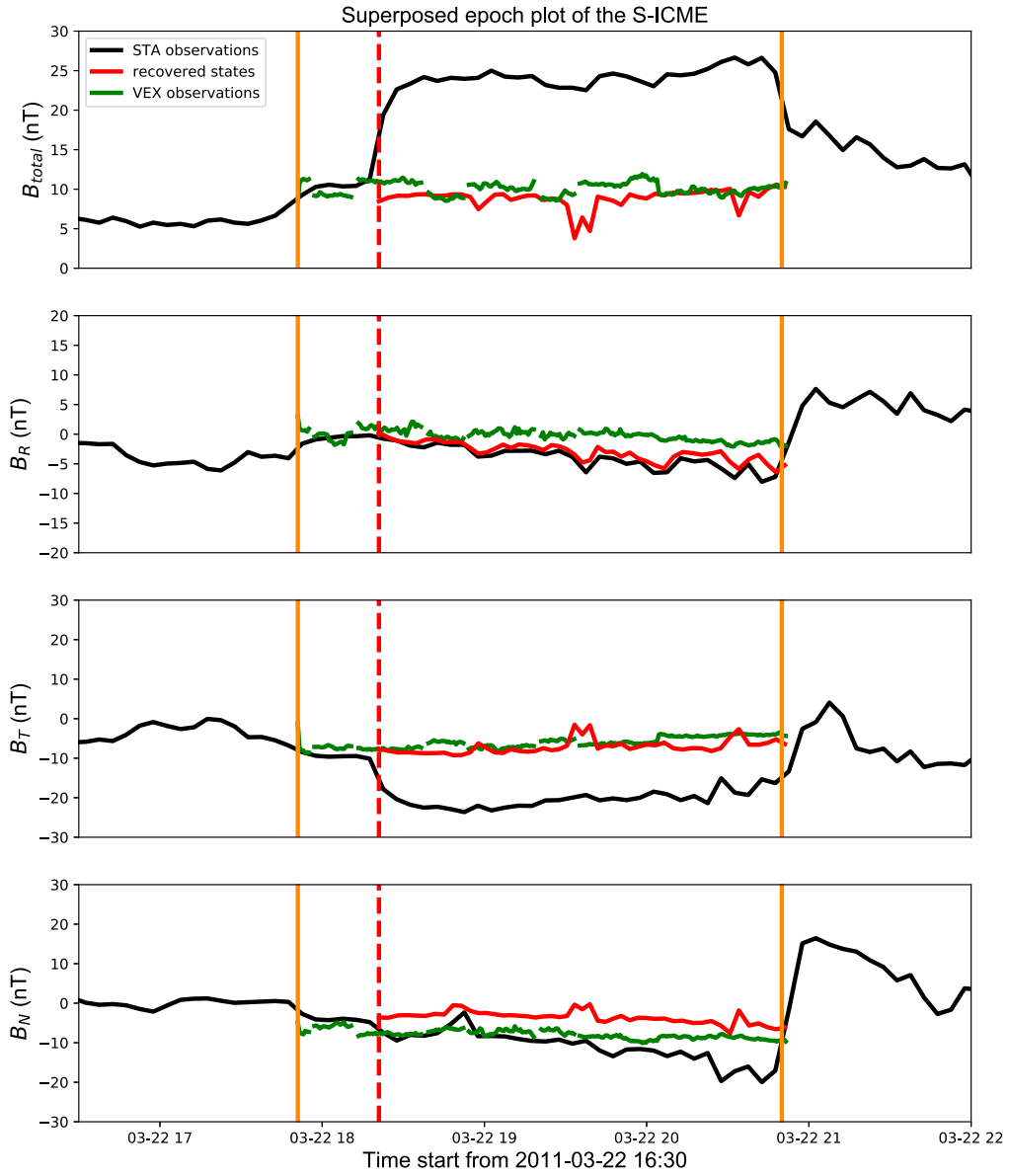

Figure 4. Superposed epoch plot of the ICMELS observed by VEX, together with the observation and recovered state of S-ICME observed by STEREO-A.

results in a deflection of shock 2's propagation direction. It is also possible that the magnetic coplanarity method does not fit shock 2 well.

The magnetic coplanarity method is used to fit shocks at Venus because it only requires magnetic field data. This method, however, has some obvious drawbacks. Substituting different upstream and downstream intervals into the magnetic coplanarity shock fitting results in very distinct and random shock normal directions, as shown in the upper part of panel (a) in Figure 3, which exhibits the fitted $\theta_{\rm BN}$ by applying the magnetic coplanarity method to VEX observations. In contrast, because both the velocity and the magnetic field are taken into account in the mixed-mode method, the calculated shock normal directions are more stable and reliable, as shown in the upper part of panel (b). Besides, because the magnetic compression ratio is independent of the fitting method, reliable results can be obtained at both Venus and STEREO-A.

In addition to shock 2, the interaction also affects the properties of the ICMELS. As shown in Table 1, the ICMELS is observed to have a much larger magnetic field strength and shorter duration at STEREO-A than at Venus. However, if we recover the shocked part of the ICMELS at STEREO-A to the uncompressed state, we can find that the ICMELS actually expands and the magnetic field intensity decreases during the propagation. This can be seen more graphically in Figure 4. The ICMELS observed at Venus and the recovered uncompressed state of the ICMELS are shortened to the length of the ICMELS observed at STEREO-A, and the three are plotted together. The black, green, and red curves represent STEREO-A observations, VEX observations, and the recovered states, respectively. The two red solid vertical lines and the red dashed vertical line mark the ICMELS interval and the position of the shock. As can be seen from the figure, the entry of shock 2 significantly enhances the magnetic field in the ICMELS. Besides, the recovered state of the ICMELS at STEREO-A is highly consistent with the observation of the ICMELS at VEX, indicating that, while the recovery method is ideal, the result is reliable in this case.

The force-free fitting results of the ICMELS at Venus and STEREO-A, as well as that of the restored uncompressed states, are also investigated to study the changes of the

ICMELS. Table 1 summarizes some important fitting parameters. Based on these parameters, we can find that the properties of the recovered ICMELS are similar to those of the ICMELS observed by VEX, except that the magnetic field strength decreases slightly. If there were no shocks, B_0 would probably drop a bit, from 18 nT to 14 nT. However, because of the compression of the shock, B_0 increased 2.4 times.

4. Summary

This work reports the formation process of a shock–ICMELS complex based on the in situ observations of two radially aligned spacecraft, VEX and STEREO-A. The shock and the ICMELS are isolated near Venus, but as they approach STEREO-A, the shock almost reaches the front end of the ICMELS and forms a shock–ICMELS complex structure. The changes in the properties of the ICMELS and shock due to the interaction are further analyzed. The propagation inside ICMELS significantly weakens the shock, reducing its magnetic compression ratio from 2.4 to 2.0. Given that the average magnetic compression ratio of the shock only decreases from 2.1 at Venus to 2.0 at 1 au, we can see that the weakening of shock 2 is more significant. In addition, due to the interaction with the shock, the ICMELS is significantly shortened and its magnetic field strength is increased markedly.

Based on multispacecraft in situ measurements, we demonstrate the formation and evolution of the shock–ICMELS complex structure. This kind of multipoint observation allows us to develop a more physical understanding of the interacting CMEs. Recently, Wang et al. (2020) proposed the "Solar Ring" mission, which will deploy three detectors at a separation angle of about 120° in the ecliptic plane to observe and study the Sun and interplanetary space from multiple perspectives. Combined with the "Solar Ring" mission and various planetary exploration satellites, most CMEs will be observed by multiple spacecraft during the propagation. This will greatly improve our understanding of the evolution of CMEs and CME complex structures.

We acknowledge the use of data from SOHO, STEREO, and Venus Express. This work is supported by grants from the Strategic Priority Program of CAS (XDB41000000), NSFC (42004143, 42188101, 41774178, 41904151, 42174213), and the Fundamental Research Funds for the Central Universities (WK2080000140).

ORCID iDs

Mengjiao Xu https://orcid.org/0000-0002-2924-7520
Chenglong Shen https://orcid.org/0000-0002-3577-5223
Can Wang https://orcid.org/0000-0002-2865-4626
Yutian Chi https://orcid.org/0000-0001-9315-4487
Zhihui Zhong https://orcid.org/0000-0002-5627-2377
Yuming Wang https://orcid.org/0000-0002-8887-3919

References

Abraham-Shrauner, B., & Yun, S. H. 1976, JGR, 81, 2097
Barabash, S., Sauvaud, J.-A., Gunell, H., et al. 2007, P&SS, 55, 1772
Burlaga, L. F., Plunkett, S. P., & St. Cyr, O. C. 2002, JGRA, 107, 1266
Farrugia, C. J., Jordanova, V. K., Thomsen, M. F., et al. 2006, JGRA, 111, A11104
Gonzalez, W. D., Joselyn, J. A., Kamide, Y., et al. 1994, JGR, 99, 5771
Good, S. W., & Forsyth, R. J. 2016, SoPh, 291, 239
Gopalswamy, N., Makela, P., Akiyama, S., Yashiro, S., & Thakur, N. 2015, SunGe, 10, 111
Gopalswamy, N., Yashiro, S., Kaiser, M. L., Howard, R. A., & Bougeret, J.-L. 2001, JGR, 106, 29219
Janvier, M., Winslow, R. M., Good, S., et al. 2019, JGRA, 124, 3238
Kaiser, M. L., Kucera, T. A., Davila, J. M., et al. 2008, SSRv, 136, 5
Kamide, Y., Baumjohann, W., Daglis, I. A., et al. 1998, JGR, 103, 17705
Kilpua, E. K. J., Jian, L. K., Li, Y., Luhmann, J. G., & Russell, C. T. 2012, SoPh, 281, 391
Kilpua, E. K. J., Lumme, E., Andreeova, K., Isavnin, A., & Koskinen, H. E. J. 2015, JGRA, 120, 4112
Lepping, R. P., Burlaga, L. F., Szabo, A., et al. 1997, JGR, 102, 14049
Lugaz, N., Farrugia, C. J., Smith, C. W., & Paulson, K. 2015, JGRA, 120, 2409
Lugaz, N., Manchester, W. B. I., Roussev, I. I., Tóth, G., & Gombosi, T. I. 2007, ApJ, 659, 788
Lugaz, N., Temmer, M., Wang, Y., & Farrugia, C. J. 2017, SoPh, 292, 64
Lundquist, S. 1950, Ark. Fys., 2, 361
Rouillard, A. P., Sheeley, N. R., Tylka, A., et al. 2012, ApJ, 752, 44
Salman, T. M., Winslow, R. M., & Lugaz, N. 2020, JGRA, 125, e27084
Schmidt, J. M., & Cargill, P. J. 2004, AnGeo, 22, 2245
Scolini, C., Chané, E., Temmer, M., et al. 2020, ApJS, 247, 21
Shen, C., Chi, Y., Wang, Y., Xu, M., & Wang, S. 2017, JGR, 122, 5931
Shen, C., Wang, Y., Wang, S., et al. 2012, NatPh, 8, 923
Shen, C., Xu, M., Wang, Y., Chi, Y., & Luo, B. 2018, ApJ, 861, 28
Srivastava, N., Mishra, W., & Chakrabarty, D. 2018, SoPh, 293, 5
Svedhem, H., Titov, D. V., McCoy, D., et al. 2007, P&SS, 55, 1636
Titov, D. V., Svedhem, H., Koschny, D., et al. 2006, P&SS, 54, 1279
Tsurutani, B. T., Gonzalez, W. D., Tang, F., Akasofu, S. I., & Smith, E. J. 1988, JGR, 93, 8519
Vandas, M., Fischer, S., Dryer, M., et al. 1997, JGR, 102, 22295
Wang, C., Xu, M., Shen, C., Chi, Y., & Wang, Y. 2021, ApJ, 912, 85
Wang, Y., Ji, H., Wang, Y., et al. 2020, ScChE, 63, 1699
Wang, Y., Shen, C., Liu, R., et al. 2018, JGRA, 123, 3238
Wang, Y., Shen, C. L., Wang, S., & Ye, P. Z. 2003a, GeoRL, 30, 2039
Wang, Y. M., Ye, P. Z., & Wang, S. 2003b, JGRA, 108, 1370
Xiong, M., Zheng, H., Wang, Y., Wang, S., & Wu, S. T. 2006, JGR, 111, 11102
Xu, M., Shen, C., Chi, Y., et al. 2019, ApJ, 885, 54
Zhang, J., Richardson, I., Webb, D., et al. 2007, JGRA, 112, A10102
Zhang, T. L., Baumjohann, W., Delva, M., et al. 2006, P&SS, 54, 1336